

# Dynamical Response of Nanomechanical Oscillators in Immiscible Viscous Fluid for in vitro Biomolecular Recognition

Jerome Dornigac<sup>1,2</sup>, Agnieszka Kalinowski<sup>3</sup>, Shyam Sunder Erramilli<sup>1,3</sup>, Prithraj Mohanty<sup>1</sup>

<sup>1</sup> Department of Physics, Boston University, 590 Commonwealth Avenue, Boston, MA 02215

<sup>2</sup> College of Engineering, Boston University, 44 Cummington Street, Boston, MA 02215

<sup>3</sup> Department of Biomedical Engineering, Boston University, 48 Cummington Street, Boston, MA 02215

(Dated: May 4, 2021)

Dynamical response of nanomechanical cantilever structures immersed in a viscous fluid is important to in vitro single-molecule force spectroscopy, biomolecular recognition of disease-specific proteins, and the detection of microscopic dynamics of proteins. Here we study the stochastic response of biofunctionalized nanomechanical cantilevers beam in a viscous fluid. Using the fluctuation-dissipation theorem we derive an exact expression for the spectral density of the displacement and a linear approximation for the resonance frequency shift. We find that in a viscous solution the frequency shift of the nanoscale cantilever is determined by surface stress generated by biomolecular interaction with negligible contributions from mass loading.

PACS numbers: 81.07.-b, 45.10.-b, 83.10.Mj, 82.70.Dd

From single-molecule force spectroscopy [1] to biomolecular recognition of disease-specific proteins such as cancer antigens [2], micron-sized cantilevers have proved to be fundamental to the ultrasensitive detection of small forces. Usually, forces are detected by measuring the deflection of the cantilever. In the dynamic case, the shift in the resonance frequency of the cantilever is used to infer the magnitude of the force. Micromachining techniques now enable commercial production of such cantilevers with dimensions on the order of 100 nm as well as their routine use in force spectroscopy.

Decreasing the cantilever dimensions to sub-micron or nanometer scales increases the resonance frequency to the megahertz-gigahertz range. The resultant increase in the dynamic range and the measurement speed can provide a better tool for probing single molecules. This could be also used for more sensitive bioimaging techniques and monitoring real-time binding kinetics of ligand-protein binding as well as the energy landscape of the molecular bonds at their true characteristic time scales. For biomolecular recognition in a viscous fluid, force sensitivity can be increased by decreasing the effective viscous damping. Nanoscale cantilevers are hence expected to have dramatically enhanced force sensitivity as smaller cantilevers have lower viscous damping.

In spite of the obvious importance of nanomechanical cantilevers for ultrasensitive in vitro force detection, there is no widely-accepted description that relates resonance frequency change to concentration or mass-loading, over the entire range of viscosity, relevant to biomolecular recognition in viscous fluids. In this Letter, we derive an exact expression that takes into account the hydrodynamics of the beam in a continuum approximation with axial loading. We find that, in air, the first mode of the nanoscale cantilever is more sensitive to surface stress than the higher order modes. The frequency shift is primarily determined by surface stress in the first

mode, where the mass-loading effects become relevant for higher order modes. More importantly, we find that, in a viscous solution such as water, frequency shift is dominated by surface stress and not mass loading, as generally expected.

Model: In standard fluid dynamics, an inviscid model is typically a valid assumption. However, nanoscale cantilevers have Reynolds numbers less than one, therefore viscous effects become dominant [3]. Proper inclusion of viscous effects is characterized as being in the Stokes-Purcell Regime of fluid flow.

Neglecting rotatory inertia, shear deformation and internal damping, the equation of motion for the deflection  $y(x;t)$  of a beam with length  $L$ , width  $b$  and thickness  $d$ , immersed in a fluid at temperature  $T$  and loaded by a constant axial force  $S$ , is given by [12]

$$EI \frac{\partial^4 y}{\partial x^4} - S \frac{\partial^2 y}{\partial x^2} + (\rho A) \frac{\partial^2 y}{\partial t^2} = f_h(x;t) + f_{th}(x;t): \quad (1)$$

$E$  and  $I$  are the Young's modulus and moment of inertia of the (coated) beam, respectively.  $f_h(x;t)$  is the hydrodynamic loading due to the motion of the fluid around the beam and  $f_{th}(x;t)$  is a Langevin-type force per unit length responsible for the thermalization of the beam. The linear mass (mass per unit length) of the system  $\rho(x)$  consists of the linear mass of the beam  $\rho_b$ , and the linear mass of the trapped biomolecules  $\rho_1(x)$ . The axial load  $S$  introduced in (1) describes the mutual interaction of biomolecules adsorbed on the beam [11]. The boundary conditions for Eq. (1) are given by  $y(0;t) = y^0(0;t) = 0$ ,  $y^0(L;t) = 0$  and  $EI y^{(3)}(L;t) = S y^0(L;t)$ , where primes denote spatial derivatives [12].

At higher concentrations, the biomolecules form a uniform layer with mass  $\rho_1$  and thickness  $h$  so that

$$\rho(x) = \rho_b + \rho_1 = \text{constant}: \quad (2)$$

The mutual interaction of biomolecules within the layer is modeled by taking into account the stress they generate

on the coated surface of the beam. As shown in ref.[2], this stress enables the bending of the silicon-nitride microcantilevers with length to thickness ratio  $L=d$ , ranging from  $10^2$  to  $10^3$ . The resulting static deflection, on the order of a few tenths of microns, is related to surface stress by Stoney's formula [10]. However, for the silicon nanomechanical cantilevers under investigation here ( $L=d \approx 50$ ), Stoney's formula typically yields angstrom-level bendings ( $10^{-5}L$ ). So these nanocantilevers remain almost straight under the influence of surface stress. Nevertheless, as shown in [11], this stress induces an effective axial load,  $S = \sigma L$ , that must be included in Eq. (1). In vacuum, such a model has been studied in ref.[13].

In addition, biomolecular interaction on the surface results in an effective Young's modulus of the layer  $E_1$  [see ref.[7]]:

$$EI = E_b I_b + E_1 I_1' = E_b b d^3/12 + E_1 h b d^2/4: \quad (3)$$

$E_b I_b$  and  $E_1 I_1'$  are the respective bending rigidities of the beam and the layer (the last equality holds when  $h = d$ ). In the opposite limit, biomolecules with mass sparsely scattered over the beam at locations  $x_i$ , result in

$$y(x) = y_b + y_1(x) = y_b + m \sum_i y(x_i); \quad x_i \in [0; L]: \quad (4)$$

If the average spacing is large compared to their size, their mutual interaction is negligible and  $S = 0$ . Considering that their presence does not substantially affect the moment  $I_b$  of the beam, the bending rigidity of the whole system is the same as for an unloaded beam,  $EI = E_b I_b$ .

Equations of Motion: To solve equation (1), we expand the deflection  $y(x;t)$  and the force densities  $f_n(x;t)$  and  $f_{th}(x;t)$  in terms of the modes of the bare beam, defined as the beam without the added mass ( $y_1(x) = 0$ ) though it includes the tension  $S = \sigma L$ :

$$y(x;t) = \sum_{n=1}^{\infty} Y_n(t) \phi_n(x); \quad x = L: \quad (5)$$

Similar expressions hold for the force densities. The eigenmodes  $\phi_n(x)$  satisfy the following conditions:

$$\begin{aligned} \phi_n^{(iv)}(x) - \omega_n^4 \phi_n(x) &= 0; \quad \omega_n^2 = L^3 EI; \\ \phi_n(0) = \phi_n'(0) = \phi_n''(L) = 0; \quad \phi_n'''(L) = \phi_n''(L): \end{aligned} \quad (6)$$

The self-adjointness of (6) makes them orthonormal:  $\int_0^L \phi_n(x) \phi_m(x) dx = \delta_{nm}$ . From Eq. (6), the eigenvalues  $\omega_n$  are the successive positive roots of

$$1 + (1 + \omega_n^2) \cosh \omega_n L \cos \omega_n L + \omega_n \sinh \omega_n L \sin \omega_n L = 0 \quad (7)$$

where  $\omega_n = (2n-1)\pi/2L$  and  $\omega_n = n\pi/L$  for  $n=1, 2, \dots$ . Note that, for  $\omega_n = (2n-1)\pi/2L$ , Eq. (7) reduces to the usual clamped-free equation,  $1 + \cos \omega_n L \cosh \omega_n L = 0$ . As  $\omega_n L \rightarrow \infty$  for large  $n$ , eigenvalues for which  $\omega_n L \rightarrow \infty$  are essentially independent of the surface stress.

Let  $y_1(x) = y_b + y_1(x)$ . Using (5), Eq. (1) reduces to

$$M \ddot{y}_n(t) + k_n \dot{y}_n(t) + \sum_{j=1}^{\infty} \gamma_{nj} y_j(t) = F_{n,th}(t) + F_{n,r}(t): \quad (8)$$

$M = \rho_b L$  is the mass of the beam and  $F_{n,th}(t) = L f_{n,th}(t)$ . The effective stiffness of mode  $n$  is

$$k_n = EI \omega_n^4 = L^3: \quad (9)$$

The real and symmetric matrix has components

$$\gamma_{nj} = L \int_0^L \phi_n(x) \phi_j(x) dx: \quad (10)$$

If  $y_1(x) = y_b$ , then  $\dot{y}_1 = M_1 \dot{1}$ , where  $1$  is the identity matrix and  $M_1 = L \rho_b$  is the layer mass. Eqs. (8) decouple and the mass of modes  $y_n$  becomes the total mass of the system,  $M + M_1$ . But non-uniform mass distributions as in Eq. (4) couple the bare modes of the beam.

Taking the Fourier transform of (8) and using the expression for the hydrodynamic force [8],

$$\hat{F}_{n,th}(\omega) = M_f \omega^2 \hat{y}_n(\omega); \quad (11)$$

where  $M_f = \frac{1}{4} L \rho_f b^2$  is the mass of the fluid loading the beam, and  $\hat{y}_n(\omega) = y_r(\omega) + i y_i(\omega)$  is a complex "hydrodynamic function" discussed in detail in [4], we obtain

$$(\hat{y}_n(\omega))_i = \hat{F}_{th}(\omega)_i: \quad (12)$$

Vectors  $\hat{y}_i$  are column vectors with components  $y_i$ ;  $i \in N$ . The nonhermitian matrix  $\hat{F}_{th}$  is given by

$$\hat{F}_{th}(\omega) = \hat{F}_{th}(\omega)^\dagger \sim \hat{F}_{th}(\omega): \quad (13)$$

where

$$\begin{aligned} \hat{F}_{th}(\omega)_{nj} &= [k_n \omega^2 (M_f(\omega) + M_n)] \gamma_{nj} \\ \hat{F}_{th}(\omega)_{nj} &= \gamma_{nj} (1 - \gamma_{nj}); \quad M_n = M + \rho_n n: \end{aligned}$$

Spectral Densities: As the dissipative (complex) part of the hydrodynamic function is frequency-dependent, we apply the generalized fluctuation-dissipation theorem [9] to derive the power spectrum matrix of the stochastic forces  $F_{n,th}$ ,  $S_{F_{n,th}}(\omega) = \overline{\hat{F}_{th}(\omega) i \hat{F}_{th}(\omega)^\dagger}$  (the over-line denotes thermal averaging, the superscript  $s$  refers to the spectral density and  $\hat{F}_{th}^\dagger$  is the hermitian conjugate of  $\hat{F}_{th}$ ):

$$S_{F_{n,th}}(\omega) = \frac{kT}{i!} y(\omega) \quad (\omega) = 2kT M_f \omega^2 \phi_n(\omega) \phi_n^\dagger(\omega): \quad (14)$$

where  $k$  is the Boltzmann constant and  $T$  the temperature. In components, this yields

$$\overline{\hat{F}_{n,th}(\omega) \hat{F}_{p,th}^\dagger(\omega)} = 2kT M_f \omega^2 \phi_n(\omega) \phi_p^\dagger(\omega): \quad (15)$$

Notice that this expression does not depend on  $\omega$ . It is the same as for a bare beam. As seen above, the stochastic forces acting on distinct modes are uncorrelated. Nevertheless, their power spectrum cannot be assumed to be constant, contrary to the assumption in ref. [4], as the dissipative part of the hydrodynamic function is frequency-dependent. Eq. (15) is the generalization of the expression derived by Paul and Cross for a single cantilever mode [6]. Now, inverting (12), we obtain

$$\hat{y}(t)_i = \hat{F}_{th}(t)_i; \quad \hat{F}_{th}(t) = \hat{F}(t) \quad (16)$$

and  $\hat{y}(t)_i \hat{y}(t)_j = \hat{F}_{th}(t)_i \hat{F}_{th}(t)_j \hat{y}(t)$ . Spectral averaging the latter and using (14), we find the power spectrum matrix of the deflection modes

$$S_{\hat{y}}(\omega) = 2kTM_f \hat{F}_i(\omega) \hat{F}_j(\omega)^* \quad (17)$$

Introducing  $\hat{y}_i$  with components  $\hat{y}_n(\omega)$ , the Fourier transform of the deflection (5) reads  $\hat{y}(x; \omega) = \sum \hat{y}_n(\omega) \hat{F}_n(x)$  and using (17), we find its spectral density to be

$$\overline{\hat{y}(x; \omega) \hat{y}^*(x'; \omega)} = 2kTM_f \hat{F}_i(\omega) \hat{F}_j(\omega)^* \hat{y}_i \hat{y}_j \quad (18)$$

The total mass of the particles trapped on the beam  $M_1$  is small compared to the mass of the beam. This justifies treating  $\hat{y}^2 \sim \hat{y}$  perturbatively provided its elements stay small compared to the diagonal elements of  $\hat{F}_0(\omega)$ . This is indeed the case provided  $M_f \hat{F}_i(\omega) \ll 4M_1$  [14]. By inverting (13), we obtain in first order in  $\hat{y}^2$

$$\hat{y} = \hat{F}_0 \hat{y}_0 + \hat{y}^2 \hat{F}_0 \sim \hat{F}_0 \hat{y}_0 + \hat{y}_0 \hat{y}_0 + O(\hat{y}^2) \quad (19)$$

where  $\hat{y}_0 = \hat{F}_0^{-1}$ . Reinstating in (18), we finally get

$$\overline{\hat{y}(x; \omega) \hat{y}^*(x'; \omega)} = 2kTM_f \hat{F}_i(\omega) \hat{F}_j(\omega)^* \sum_{n=1}^{\infty} \frac{\hat{F}_n^2(\omega)}{M_n^2 \hat{A}_n^2} + 2 \sum_{n=1}^{\infty} \sum_{p=1}^{\infty} \frac{\hat{F}_n(\omega) \hat{F}_p(\omega)^* \hat{y}_{np} < \hat{A}_p}{M_n^2 M_p \hat{A}_n^2 \hat{A}_p^2} + O(\hat{y}^2) \quad (20)$$

In this expression,  $\hat{F}_n = x=L, \hat{y}_{np}$  is given by (14) and the quantity  $\hat{A}_n = \hat{F}_0(\omega)_{nn} = M_n$  reads

$$\hat{A}_n = \omega_n^2 (1 + \hat{y}_n(\omega)) \quad (21)$$

where  $\omega_n = \sqrt{k_n/M_n}$  is the frequency in vacuum,  $\omega_n = M_f/M_n$  and  $< \hat{A}_n$  is the real part of  $\hat{A}_n$ . An expression similar to (20) can be derived for the slope of the deflection provided  $\hat{y}_j(\omega)$  is replaced by  $\hat{y}_j'(\omega)$  and the overall prefactor is divided by  $L^2$ .

Expression (20) is valid for any mass distribution  $\rho_1(x)$  along the beam. For a uniform layer with linear mass  $\rho_1$ ,  $\hat{y}_{np} = L \rho_1 \hat{y}_{np}$ , and then  $\hat{y}_{np} = 0$ . All modes have the same effective mass,  $M_n = M + L \rho_1$ , and are decoupled. Reinstating in (20), the second term vanishes and we obtain the exact spectral density of a composite

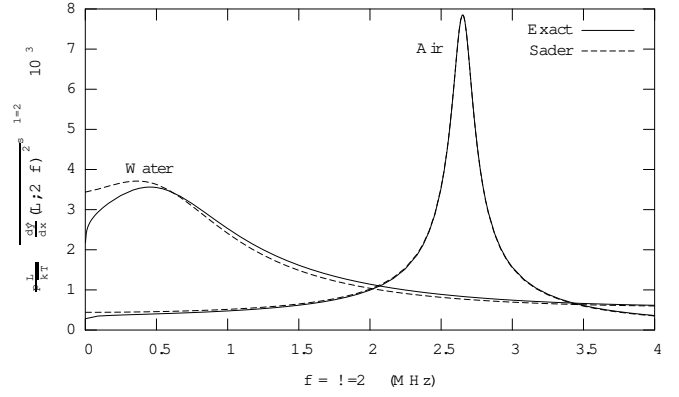


FIG. 1: Spectral density of the deflection slope for a bare silicon nanobeam in air and water (solid lines) compared to Sader's expression [4] (dashed lines).

beam consisting of the original beam plus the layer. For molecules trapped on the beam at positions  $x_i$ , the mass profile given in Eq.(4) leads to  $\hat{y}_{np} = \sum \hat{y}_n(x_i) \hat{F}_p(x_i)$  and Eq.(20) is valid up to first order in  $\hat{y}$  provided the frequency satisfies  $M_f \hat{F}_i(\omega) \ll 4M_1$ . Interestingly, if we assume  $N$  molecules to be randomly scattered along the beam in a uniform way and average  $\hat{y}_{np}$  accordingly, we find  $\overline{\hat{y}_{np} \hat{y}_{np}^*} = \sum \hat{y}_n(x_i) \hat{F}_p(x_i) \hat{y}_n^*(x_i) \hat{F}_p^*(x_i) = N \overline{\hat{y}_{np}}$ . As the total mass of the trapped molecules is small compared to the mass of the beam, in the first approximation, the average spectral density is the same as the spectral density of their average mass distribution, i.e. the spectral density of a uniform layer of mass  $Nm$ .

In Fig. 1, we compare the bare beam ( $\rho = 0$ ) spectral density of the deflection slope at the tip of a rectangular silicon nanocantilever ( $E = 160$  GPa,  $\rho = 2.33 \times 10^3$  kg/m<sup>3</sup>) to Sader's result [4] in air and water. The beam dimensions are  $d \times b \times L = 0.2 \times 0.2 \times 10$  ( $\mu$ m). From [5], at  $T = 27^\circ$  C, the viscosities are  $\eta_{air} = 1.86 \times 10^{-5}$ ,  $\eta_{water} = 8.59 \times 10^{-4}$  (kg/m/s) and the densities,  $\rho_{air} = 1.18$ ,  $\rho_{water} = 997$  (kg/m<sup>3</sup>). Although different, Sader's formula can be shown to reduce to (20) provided  $\hat{y}_j(\omega) \ll 1$ . This explains why the results are very similar in air ( $\hat{y}_j(\omega) \ll 0.06$  at resonance) while they start to differ in water ( $\hat{y}_j(\omega) \ll 0.25$  at resonance).

**Frequency Shift:** As stated earlier, when trapped molecules form a uniform layer, the exact spectral density of the beam deflection is given by

$$\overline{\hat{y}(x; \omega) \hat{y}^*(x'; \omega)} = \frac{2kTM_f \hat{F}_i(\omega) \hat{F}_j(\omega)^*}{(M + M_1)^2} \sum_{n=1}^{\infty} \frac{\hat{F}_n^2(\omega)}{\hat{A}_n^2}; \quad (22)$$

where  $M_1$  is the mass of the layer and where  $\hat{A}_n$  is given in Eq.(21) with  $M_n = M + M_1$ . When the peaks of Eq.(22) are sharp enough, the hydrodynamic function is almost constant in their vicinity and the resonant frequency sat-

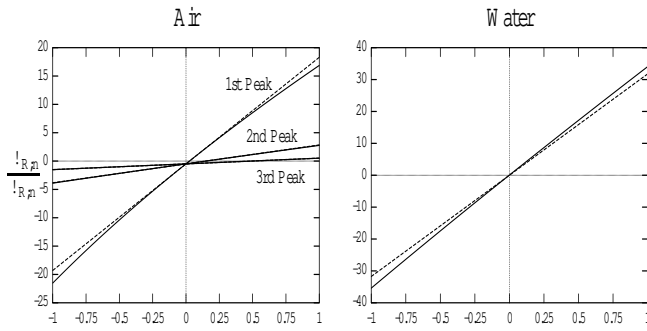


FIG. 2: Relative frequency shift (in %) in air and water vs the dimensionless stress,  $\sigma = L^3 = EI \cdot M_1 = M = 100$  and  $E_1 = 0$ . Other parameters are the same as in Fig. 1. Solid line: exact result from Eq. (22). Dotted line: linear approximation from Eqs. (24) and (25).

is es the self-consistent equation

$$\Delta_{R,m}^2 = f(\Delta_{R,m}; M_n) k_n; \quad f = \frac{1}{3} \frac{R + \frac{P}{4R^2 + 3I^2}}{R^2 + I^2} \quad (23)$$

where  $R = M_n + M_{f_r}$ ,  $I = M_{f_i}$  and  $r_{ji} = r_{ji}(\Delta_{R,m})$ . From the expression (23), the mass and sti ness variations due to the layer,  $M$  and  $k_n$ , induce a relative frequency shift between a bare and a loaded beam :

$$\frac{\Delta_{R,m}}{\Delta_{R,m}} = \frac{1}{2} \frac{1}{\Delta_{R,m} \frac{\partial \ln f}{\partial \Delta_{R,m}}} \frac{k_n}{k_n} + \frac{\partial \ln f}{\partial M} M : \quad (24)$$

Here,  $M = M_1$  and its prefactor in (24) takes into account dissipative ( $M_{f_i}$ ) and uid mass loading ( $M_{f_r}$ ) e ects. According to (9), the two contributions to the sti ness  $k_n$  come from the bending rigidity,  $E_b I_b$ ,  $E_b I_b + E_1 I_1$ , and from the surface stress through the eigenvalue  $n(\cdot)$ . From (3) and (7), we nd

$$\frac{k_n}{k_n} = \frac{3hE_1}{dE_b} + \frac{2T_n t_n + \sigma_{0n} (T_n + t_n)}{3 \sigma_{0n} (t_n - T_n)} ; \quad (25)$$

where  $\sigma_{0n}$  is the  $n$ th root of  $\cosh(\cdot) \cos(\cdot) + 1 = 0$  and where  $T_n = \tanh \sigma_{0n}$ ,  $t_n = \tan \sigma_{0n}$ . The last term of (25) has been obtained from (7) in perturbation. It is valid when  $n^2$  and vanishes as  $n \rightarrow 1$ .

Using the same data as in Fig. 1, we display in Fig. 2 the relative frequency shift in air (left) and water (right) versus the dimensionless surface stress  $\sigma$ . The exact shift is evaluated from the spectral density (22) and compared to its linear approximation (24). The layer mass has been arbitrarily xed to 1% of the beam mass and  $E_1$  set to zero, hence the negative o set observed in air at  $\sigma = 0$ . For typical values of the surface stress,  $10^2 \text{ J m}^{-2}$  (see Wu et al. in ref. [2]),  $j \approx 1$ . In air,  $j(\Delta_{R,m}) \approx 1$ , and  $f \approx 1/M$ . Then,  $\partial \ln f / \partial M \approx -1/M$ ,  $\partial \ln f / \partial k_n \approx 0$ , and we recover

the usual frequency shift for a linear oscillator in vacuum. As seen on the left panel, the first peak is the most sensitive to  $\sigma$ . The deviation of the data from the linear result (25) indicates that the condition  $n^2$  with  $n = 1$  becomes violated. This e ect disappears for the second and third peaks that are less sensitive to  $\sigma$ . In water (right panel), a single broad peak occurs. Eq. (23) loses its accuracy but the frequency shift (24) derived from it is still acceptable. The contribution of  $\partial \ln f / \partial M$  becomes negligible while  $\partial \ln f / \partial k_n \approx -1/M$  and  $\partial \ln f / \partial \Delta_{R,m} \approx 1/M$  becomes important, hence the increase in the slope of the relative frequency shift versus  $\sigma$  in water compared to air.

In conclusion, we treat the stochastic response of bio-functionalized nanomechanical cantilevers with a generalized actuation-dissipation relation. In a viscous uid like water, the resonance frequency shift for a continuous distribution of biomolecules on the cantilever surface is dominated by surface stress rather than mass loading.

- [1] M. B. Vianiet al, Jour. Appl. Phys. 86, 2258 (1999).
- [2] G. Wu et al, Nature Biotechnology 19, 856 (2001). G. Wu et al, PNAS 98, 1560 (2001).
- [3] E. M. Purcell, Am. J. Phys. 45, 3 (1976).
- [4] J. E. Sader, J. Appl. Phys., 84, 64 (1998); C. P. Green and J. E. Sader, Jour. Appl. Phys. 98, 114913 (2005).
- [5] J. W. N. Chon and P. M. Ulvaney, J. Appl. Phys. 8, 3978 (2000).
- [6] M. R. Paul and M. C. Cross, Phys. Rev. Lett. 92, 235501 (2004). In Eq. (5) of the above paper,  $m_e$  should be replaced by  $m$ . The extra factor 2 contained in this equation as compared to our equation (15) is due to our convention to work with double-sided Fourier transform.
- [7] J. P. Gere and S. P. Timoshenko, Mechanics of Materials, (PWS Publishing Company, 1997).
- [8] L. Rosenhead, Linear Boundary Layers, p.391 (Clarendon, Oxford, 1963). We assume here that the presence of a layer of molecules binding to the beam does not a ect the hydrodynamic force.
- [9] N. Smith, J. Appl. Phys., 90 (11), 5768 (2001); J. Appl. Phys., 92 (7), 3877 (2002).
- [10] G. Stoney, Proc. Roy. Soc. of London, Series A, 82 (553), 172 (1909). J. E. Sader, J. Appl. Phys., 89 (5), 2911 (2001).
- [11] G. Y. Chen et al. J. Appl. Phys., 77 (8), 3618 (1995). P. Muller and R. Kem, Surf. Sci. 301 (1-3), 386 (1994).
- [12] J. L. Humar, Dynamics of Structures, p. 654 (Prentice Hall, New Jersey, 1990).
- [13] P. Lu et al, Mater. Phys. Mech 4, 51 (2001). Q. Ren and Y. P. Zhao, Microsystems Technologies 10, 307 (2004).
- [14] As  $n \rightarrow 1$ ,  $\Delta_{R,m} \rightarrow 0$  when  $n \rightarrow 1$ ,  $M_{f_i} \rightarrow 4M_1$  is violated at some critical frequency beyond which Eq. (19) does not hold. A "non-perturbative" treatment of the inversion of  $(\Delta_{R,m})$  is then in order. It can be done approximately by analytically inverting the 2x2 or 3x3 sub-block of  $(\Delta_{R,m})$  surrounding the small diagonal element.